Ultrasonic wireless power links for battery-free condition monitoring in metallic enclosures

PLEASE CITE THE PUBLISHED VERSION

https://doi.org/10.1016/j.ultras.2021.106395

PUBLISHER

Elsevier BV

VERSION

AM (Accepted Manuscript)

PUBLISHER STATEMENT

This paper was accepted for publication in the journal Ultrasonics and the definitive published version is available at https://doi.org/10.1016/j.ultras.2021.106395

Ultrasonic Wireless Power Links for Battery-Free Condition Monitoring in Metallic Enclosures

Hailing Fu[a], Jing Rao[b,*], Mohammad S. Harb[c], Stephanos Theodossiades[a]

[a] *Wolfson School of Mechanical, Electrical and Manufacturing Engineering, Loughborough University, LE11 3TU, UK*
[b] *Chair of Computational Modeling and Simulation, Technical University of Munich, Arcisstr. 21, 80333 Munich, Germany*
[c] *Laboratory of Smart Structures and Structural Integrity, Department of Mechanical Engineering, American University of Beirut, Beirut, Lebanon*

Abstract

This paper presented a novel ultrasonic wireless power link (UWPL) to provide power supply for embedded condition monitoring of enclosed metallic structures, where recharging or replacing batteries can be problematic. Two piezoelectric transducers are adopted to establish the wireless power links, within which one transducer is used to generate ultrasonic waves and the other is to receive the transferred ultrasonic energy and to energize the associated embedded condition monitoring units. A power management solution is established to regulate the receiver output into a constant voltage suitable for sensing application. A theoretical model was established to understand the UWPL dynamics and to analyze the energy budget balance between the UWPL and the sensing power demands. A finite element model was built to validate the proposed idea. The UWPL was then experimentally implemented using two piezoelectric transducers and tested in aluminium plates with different thickness. A power management sub-system was developed and tested for sensing applications. An output power of 1.73 mW was obtained on a 1.5 kΩ resister with the input voltage of 15 V at 42.6 kHz through a 6 mm-thick aluminium plate. Sufficient power can be transferred over a large distance via metallic structures, showing the capability in implement-

*This is the corresponding author.

Email addresses: h.fu@lboro.ac.uk (Hailing Fu), jing.rao@tum.de (Jing Rao), mh243@aub.edu.lb (Mohammad S. Harb), s.theodossiades@lboro.ac.uk (Stephanos Theodossiades)

ing battery-free condition monitoring of enclosed metallic structures, such as petroleum pipelines, engines, and aluminium airframe.

Keywords: Ultrasonic, Wireless Power Links, Piezoelectric Transducers, Metallic Enclosures

1. Introduction

Structural integrity and operation safety have been gaining increasing attention for many applications, ranging from civil infrastructure to industry machinery [1, 2, 3]. Condition monitoring [4] or structural health monitoring [5] using embedded sensors has been used to collect critical operational data to assess the operating conditions or safety. In order to achieve distributed large-scale monitoring, a concept called ”smart dust” using wireless sensor networks (WSN) has been proposed [6, 7], where sensors are included within a WSN and operational data from individual sensors are reported to the central coordinator via different wireless communication mechanisms. For instance, Yuan *et al.* developed a wireless impact monitoring network for aircraft composite structures, in which impact event on large-scale composite structures are monitored by piezoelectric transducers and the monitored data are transferred to the center for post-processing by the IEEE 802.15.4 protocol [8]. Similarly, Ozdagli *et al.* presented a low-cost WSN to monitor real-time dynamic displacement of mechanical systems [9].

However, in such WSNs, one of the critical challenges is sustainable power supply. Currently, most of the wireless sensors are powered by conventional batteries that are bulky and require regular replacement or recharging [10]. This is impractical or costly in many applications where sensors are widely distributed or in some inaccessible locations, such as enclosed machines or engines [11, 12]. There are mainly two research streams in addressing this challenge, including energy harvesting [13, 14, 15, 16] and wireless power transfer [17, 18, 19, 20]. Energy harvesting is a technology that converts the ambient energy sources from the environments into electricity to power sensors. A good example is a vortex-induced vibration energy harvester that harnesses fluid flow energy for sensing application [21]. While energy harvesting provides a sustainable solution for sensing applications, it is highly dependent on the availability of the environmental energy sources, such as the variation of light during day and night [22]. The advantages of energy harvesting or the self-powered sensing capability will be compromised in cases where available energy sources vary significantly.

Wireless power transfer (WPT) is another mechanism to provide reliable power supply to wireless sensors. Inductive power transfer (IPT) is the straightforward solution, where electromagnetic waves are generated in coils by applying alternating currents in the coils. A coil pair including a transmitter and a receiver, is used to implement power links between two unconnected objects [23]. This technology has been used widely in charging implantable devices [24], electric vehicles [25], cellphones [26] and drones [27]. Biomedical applications are one of the major applications for IPT due to the difficulties in using battery-powered implants [28]. Wang *et al.* developed a resonance-based wireless power delivery system with a ⌀22 mm receiving implantable coil [29]. 80 mW power was received by the implant over 20 mm with the input power being 0.1 W. Ahmadi *et al.* presented a method to realize inductive power and data transmission simultaneously using inductive coils and the frequency-shift keying mechanism [30]. 25% power transfer efficiency and 126 mW delivered power were realized with a 6 mm air gap. In addition to biomedical applications, IPT has also been used in energizing battery-less drones. Arteaga *et al.* developed an inductive power link between a power pad and a battery-less drone with a receiving coil [27]. The drone was sufficiently charged and operated normally without a battery. More recently, Boyle *et al.* presented an idea to use drones and IPT to deliver energy to wireless sensors in large-scale distributed sensing applications [31].

Although IPT presented excellent performance in providing wireless power links, the constraints in receiver dimensions, power transfer distance, power safety limits and heat generation [32] prompt many researchers to engage in studying ultrasonic power transfer (UPT) using piezoelectric transducers. UPT outperforms IPT when the transfer distance increases and the receiver dimension decreases [33]. For UPT, instead of using coil pairs, piezoelectric transducers are formed in pairs including one transmitter and one receiver which are used to generate and receive ultrasonic waves, respectively. This type of configuration has also been used in active sensing in structural health monitoring, where the receiver is used to sense structural responses [34]. In power transfer, biomedical implanted devices are still the major application. Charthad *et al.* developed a millimeter sized implants using UPT [35]. High delivered power (over 100 μW) was obtained in mm-sized piezoelectric receivers via human tissue over a long distance (up to 10 cm). Similar ideas have been developed to energize implantable devices in recording nervous systems [36], energizing electrical stimulators for movement restoration [37] and recharging embedded batteries in implants [38]. Investigating and optimizing UPT solutions are also contemporary research streams. Allam *et al.* studied the influence of the transducer dimension aspect ratio on the UPT performance using different theories [39]. Arrays of rod-like transducers were recommended to be better than a whole plate-shape receiver of the same dimensions. In order to compensate tissue changes (distance) between ultrasonic power links, Vihvelin *et al.* developed a method to actively adjust the transmitter actuation frequency [40]. The power transfer efficiency was maintained on a high level (20% to 27%) under tissue changes.

Another advantage of UPT over IPT is that ultrasonic waves used in UPT can penetrate enclosed metallic structures. However, this is impossible for IPT, because a metallic enclosure forms the Faraday cage in which electromagnetic waves are totally shielded. UPT, therefore, becomes a favorable solution in transferring energy via metallic structures [41, 42, 43]. For example, Kiziroglou *et al.* presented an acoustic power delivery solution for monitoring pipeline conditions using wireless sensors [44]. Instead of using through-wall power transfer, surface waves were used to transfer energy over a large distance on the pipeline surface. Ashdown *et al.* [45] presented a power and information deliver system through a metallic block. A large transfer distance was achieved, but it is worth mentioning that the tested metallic block did not form a faraday cage. Similarly studies on through-metallic structure power transfer are summarized in [46]. The other gap identified in the literature is that most of the studies focuses on the component level performance investigation, but the system-level study with the consideration of subsequent power management circuits is less investigated.

In this paper, a UPT system with piezoelectric transducers and the subsequent power management circuits to deliver energy over fully enclosed metallic structures is studied for the first time. The novelty lies in using ultrasonic devices for wireless power transfer via metallic structures and establishing the system-level solution and its associated energy budget balance analysis model. In this work, a theoretical model was established based on the classical Krimholtz, Leedom, and Matthae model to study the generated ultrasonic waves and to estimate the obtainable transferred power. A system-level model, including UPT, power management circuit and sensing subsystems was established to analyse the energy budget balance. A finite-element model was built to study the wave propagation over metallic enclosure and to validate the proposed idea. An experimental study was conducted afterwards to test the power transfer capability under different conditions. Finally, the conclusions and outlook are summarized.

2. System Design and Theoretical Modelling

2.1. Ultrasonic Power Link and Its Configuration

The system configuration of the proposed ultrasonic wireless power link (UWPL) is shown in Fig. 1(a). A piezoelectric transmitter (PZT Tx) is mounted on the surface of a metallic enclosure. The transmitter is connected to an amplifier associated with a signal generator that provides the excitation signal for the transmitter at certain frequencies and amplitudes. Being paired with the transmitter, a piezoelectric receiver (PZT Rx) is mounted inside the metallic enclosure, facing the PZT Tx. Ultrasonic waves generated by the PZT Tx penetrate the metallic enclosure and activate the PZT Rx. Electricity can be generated on PZT Rx. A power management circuit is

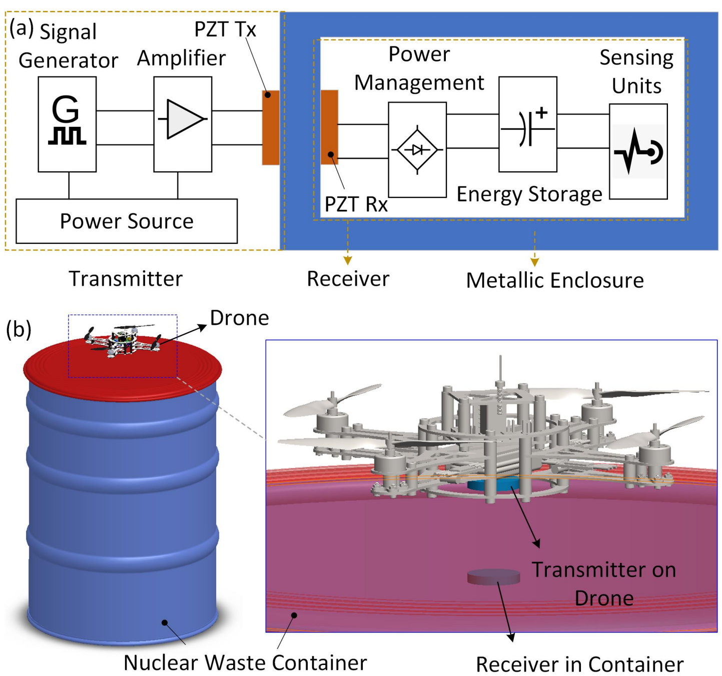

Figure 1: (a) Schematic of the ultrasonic power links and (b) a potential application demonstration in powering condition monitoring units inside metallic nuclear waste containers using drones.

connected to the PZT Rx to rectify the voltage into the direct-current form, and the generated power is then stored in a supercapacitor, before being used to power the subsequent sensing units for monitoring purposes.

Currently there is an unmet and urgent demand in monitoring a large number of nuclear containers to understand the container internal conditions and potential risks. A potential application in nuclear waste container monitoring using UWPL is illustrated in Fig. 1(b).The sensing unit is embedded inside the metallic container. These units are powered by the ultrasonic power links, where the PZT Rx is connected to the sensing units inside the container and the PZT Tx is outside. In order to realize an autonomous process without human involvement, using drones to carry the PZT Tx is a potential solution to implement ultrasonic power transfer for containers distributed over a large area. Magnetic positioners and clamps can be designed and adopted to apply sufficient pre-loads between the PZT Tx and the container and place the PZT Tx in the expected locations accurately by drones. In order to realize such systems, multi-facet research activities are necessary, nevertheless this paper will mainly focus on the UWPL over metallic enclosures.

2.2. Ultrasonic Power Link Modelling

In order to understand the system dynamics, a theoretical model is established to study the UWPL behaviours under different operation conditions. Fig 2(a) illustrates a UWPL with two piezoelectric transducers with a metallic medium. Based on the classical Krimholtz, Leedom, and Matthae (KLM) model [47], the piezoelectric transducers can be modeled using an equivalent circuit as shown in Fig 2(b). Mechanical and electrical ports are introduced to mimic the electromechanical conversion of the piezoelectric effect. Accordingly, the overall UWPL in Fig 2(a) is modelled as an electrical circuit, as shown in Fig 2(c). The effect of the metallic medium is modelled as an impedance component Z_{Medium} in series with the acoustic impedance of the piezoelectric transmitter and receiver.

X_{Tx} and X_{Rx} are the frequency-dependent admittance of the transmitter and receiver. These values become zero when the transducers operates at their resonance frequencies f_r expressed as

$$f_r = \frac{v_D}{2d}, \tag{1}$$

where v_D is the velocity of ultrasonic waves travelling in piezoelectric materials, and d is the transducer thickness. The acoustic impedance is determined

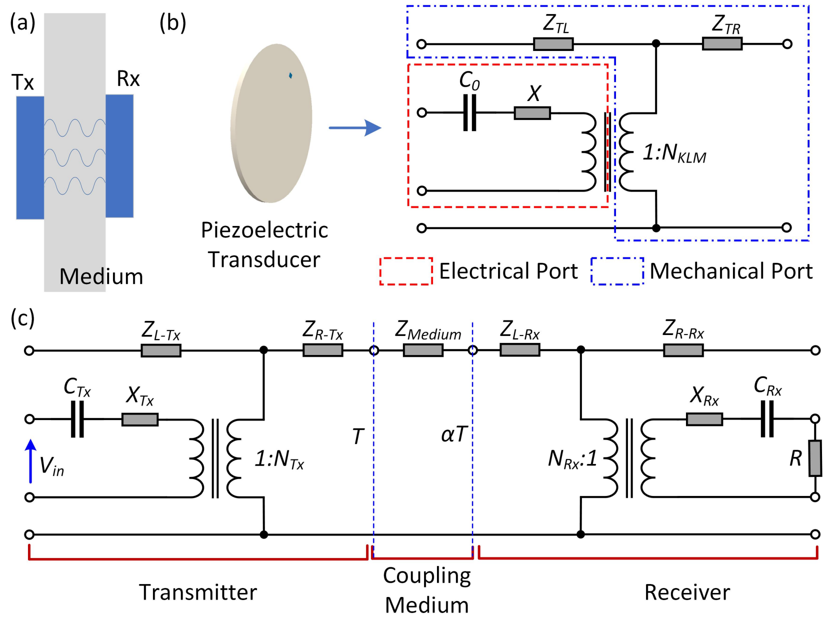

Figure 2: Ultrasonic power link models. (a) Physical model of the UWPL; (b) equivalent circuit model of piezoelectric transducers and (c) overall equivalent model of the UWPL including the transmitter, receiver and the coupling medium.

by the transducer surface A_p, and given by

$$Z_0 = \rho A_p v_D = A_p \cdot \sqrt{\rho \cdot c_{33}^D}, \tag{2}$$

where ρ is the transducer material density and c_{33}^D is the material elastic stiffness in the open-circuit condition. As shown in Fig. 2(b), C_0 is the transducer capacitance and is expressed as

$$C_0 = \frac{\epsilon_{33}^S \cdot \epsilon_0 A_p}{d}, \tag{3}$$

where ϵ_0 is the electric constant in free space, ϵ_{33}^S is the material relative permittivity of the piezoelectric transducer, and d is the transducer thickness. The electromechanical conversion is represented using an ideal transformer, as shown in Fig. 2(b). Based on the piezoelectric coupling dynamics, the turn ratio can be written as

$$N_{KLM} = \frac{1}{2\left(\frac{h_{33}}{\omega Z_0}\right)} \csc\left(\frac{\beta t}{2}\right), \tag{4}$$

where β is the wave number, t is time, ω is the operation frequency, and h_{33} is the piezoelectric pressure constant given by

$$h_{33} = k_t \frac{c_{33}^D}{\epsilon_{33}^S \cdot \epsilon_0}, \tag{5}$$

where k_t is the electromechanical coupling factor. The impedance components of the KLM model in Fig. 2(b) can be written as

$$Z_{TL} = Z_0 \left[\frac{Z_L \cos\left(\frac{\beta t}{2}\right) + iZ_0 \sin\left(\frac{\beta t}{2}\right)}{Z_0 \cos\left(\frac{\beta t}{2}\right) + iZ_L \sin\left(\frac{\beta t}{2}\right)} \right], \tag{6}$$

$$Z_{TR} = Z_0 \left[\frac{Z_R \cos\left(\frac{\beta t}{2}\right) + iZ_0 \sin\left(\frac{\beta t}{2}\right)}{Z_0 \cos\left(\frac{\beta t}{2}\right) + iZ_R \sin\left(\frac{\beta t}{2}\right)} \right], \tag{7}$$

$$X = iZ_0 \left(\frac{h_{33}}{\omega Z_0} \right)^2 \sin\left(\frac{\beta t}{2} \right), \tag{8}$$

where Z_L and Z_R are the the port impedance on the left and right sides, respectively.

Assuming the system operates at the resonant frequency, the output power that the load R receives can be obtained using the Thevenin equivalent model [48], which can be expressed as

$$P_{out} = \frac{1}{2C_{Rx}} \left(\alpha T \cdot N_{Rx} \cdot \frac{R}{R + Z_{out}} \right)^2 \cdot f_r, \tag{9}$$

where N_{Rx} is the equivalent transformer ratio, T is the equivalent electromotive force generated by the transmitter, α is the medium attenuation ($\alpha = e^{-2ux}$, u is the attenuation ratio, and x is the wave travel distance) and Z_{out} is the output impedance of the receiver and is given by $Z_{out} = 1/j\omega C_{Rx}$ (C_{Rx} is the receiver capacitance). The theoretical power transfer efficiency η_t can be obtain using the above theory as

$$\eta_t = \left| \frac{P_{out}}{P_{in}} \right| = \frac{\left(\alpha T \cdot N_{Rx} \cdot \frac{R}{R+Z_{out}} \right)^2}{C_{Tx} C_{Rx} V_{in}^2}, \tag{10}$$

where P_{in} is the input power to the transmitter and is given by $P_{in} = \frac{1}{2} C_{Tx} \cdot V_{in}^2 \cdot f_r$, and V_{in} is the input voltage. According to Eq. (9) and (10), the output power and power transfer efficiency are highly related to the square of the attenuation ratio α^2, which means with the increase of the transfer distance d, the obtainable power and the efficiency from the receiver will decrease dramatically. In order to maintain the power supply capability for sensing applications, increasing the equivalent electromotive force T or enhancing the equivalent transformer ratio N_{Rx} of the receiver are the potential solutions.

2.3. Power Management Solutions for Battery-Free Sensing

Since the output power from the receiving transducer is in an alternating current (AC) form, it is necessary to convert it into the direct current (DC) form and stabilize the output voltage at a constant level (e.g. 3 V). A diagram for the power management circuit (PMC) and sensing coordination is illustrated in Fig. 3(a), showing the key function blocks. The bridge rectifier converts the AC power into DC, and the subsequent DC-DC converter produces a stable and constant output for energy storage and powering sensing electronics. For energy storage, super-capacitors and rechargeable batteries are the options with the trade-off among energy density, charging and discharging rate and current supplying capability [49]. Super-capacitors are ideal in this application due to the better current supplying capability. Another critical block is the voltage comparator module which monitors the voltage status on the super-capacitor. If a sufficient level of voltage is accumulated, an enabling signal will be provided to notify the subsequent sensing applications that the power supply is ready. It is worth noting that while

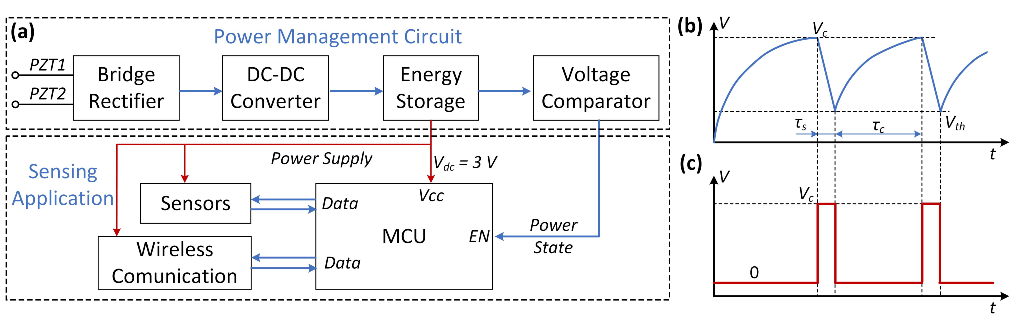

Figure 3: Power management circuit and energy storage for energizing embedded sensing applications. (a) Function blocks for PMC and sensing; (b) charging and discharging dynamics of the energy storage and (c) power readiness indicator generated by the voltage comparator module.

the PMC manages the received energy from the PZT Rx, the whole PMC is powered by this energy without using any batteries.

From the sensing application side, an event-triggered mechanism is necessary to make the system operate with different power consuming modes to not only realize the demanded sensing functions but also achieve an energy balance between the sensing power consumption and the power transfer capability. In order to better understand the energy balance dynamics and to analyze the power transfer demands, an energy balance model is established here with the consideration of energy transfer capability, PMC efficiency, energy storage capacity and sensing power consumption. Assuming the received voltage at the receiver end is V_{out}, the available energy for the PMC is

$$P_c^{in} = \frac{1}{2} C_{Rx} \cdot V_{out}^2 \cdot f_r. \tag{11}$$

Due to the energy losses from the PMC, the power available for sensing applications will be less than P_c^{in}. Assuming conversion efficiency of η_c, the power delivered to the power storage is $\eta_c \cdot P_c^{in}$. However, if the voltage on the storage drops to a certain level V_{th}, it would not be enough for the sensing application to operate normally, as shown in Fig. 3(b). This lower voltage limit V_{th} can be either determined by the voltage comparator module or the sensing subsystem. Fig. 3(c) illustrates voltage readiness indicator on the energy storage for sensing application. This indicator turns into V_c when the voltage reaches the upper limit V_c and drops to zero when the voltage on the capacitor decrease to V_{th}. In conditions where the instantaneous power transfer capability is much lower than the power consumption of the sensing units, the voltage on the energy storage will drop sharply once the sensing unit is on, as shown in Fig. 3(b). The usable energy in one discharging cycle for sensing is

$$E_s = \frac{1}{2} C_s \left(V_s^2 - V_{th}^2 \right), \tag{12}$$

where C_s is the storage capacitance and V_s is the upper voltage limit of the energy storage.

In cases when the instantaneous transferred energy is not sufficient to maintain continuous operation of the sensing systems, it is necessary that the energy demand for the sensing units are lower than the usable energy from the energy storage E_s for one discharging cycle. The energy consumption per discharging and charging cycle $(\tau_s + \tau_c)$ is the total energy consumed by all the sensing modules during both the low-power and active states. The total energy consumption per cycle as a function of the time interval between charging and discharging cycles can be written as

$$E_u = \underbrace{P_a \cdot \tau_s + P_s \cdot \tau_c}_{\text{Micro-controller unit}} + \underbrace{P_a^w \tau_a^w + P_s^w (\tau_c + \tau_s - \tau_a^w)}_{\text{Wireless module}} + \underbrace{P_{other} \cdot (\tau_s + \tau_c)}_{\text{Other modules}}, \quad (13)$$

where P_a and P_s are the power consumption of the MCU in active and sleep modes respectively, τ_s is the sensing operation duration, τ_c is the duration of the sleep mode, P_a^w and P_s^w are the power consumption of the wireless module for the active and low-power modes respectively, τ_a^w is the operation duration of the wireless module in one operation cycle, P_{other} is the average power consumed by other modules, including the comparison module. In order to realize sensing function per charging and discharging cycle, it is critical to maintain an energy budget balance between the usable energy from the capacitor E_s and the power consumption of the sensing units E_u in Eqs. (12) and (13).

3. Testing Approach

Experimental study and simulation using COMSOL Multiphysics are used to parametrically study the proposed UWPL design. The experimental and simulation details are included below.

3.1. Experimental Setup

In order to validate the proposed system, an experimental setup was established, as shown in Fig. 4. Fig. 4(a) illustrates the concepts of UWPL using two piezoelectric transducers mounted on two sides of an aluminium plate with the dimensions of 100 mm × 100 mm × 6 mm. The transducers 400EP250 from POWERWAVE were used as the transmitter and receiver. The diameter is ⌀25 mm with the center frequency of 40 kHz and capacitance of 2.4 μF. Elastic bands were used for the convenience of adjusting of transducer location and preloading level. Epoxy was not used in this study, but it would be a potential mounting solution in practice combined with other fastening mechanisms [50]. Adopting an appropriate couplant (e.g. glycerin) can potentially improve the energy transfer capability as well [51].

Fig. 4(b) presents a setup to test the capability of the UWPL in powering an embedded sensing application. The receiver was placed in a metallic

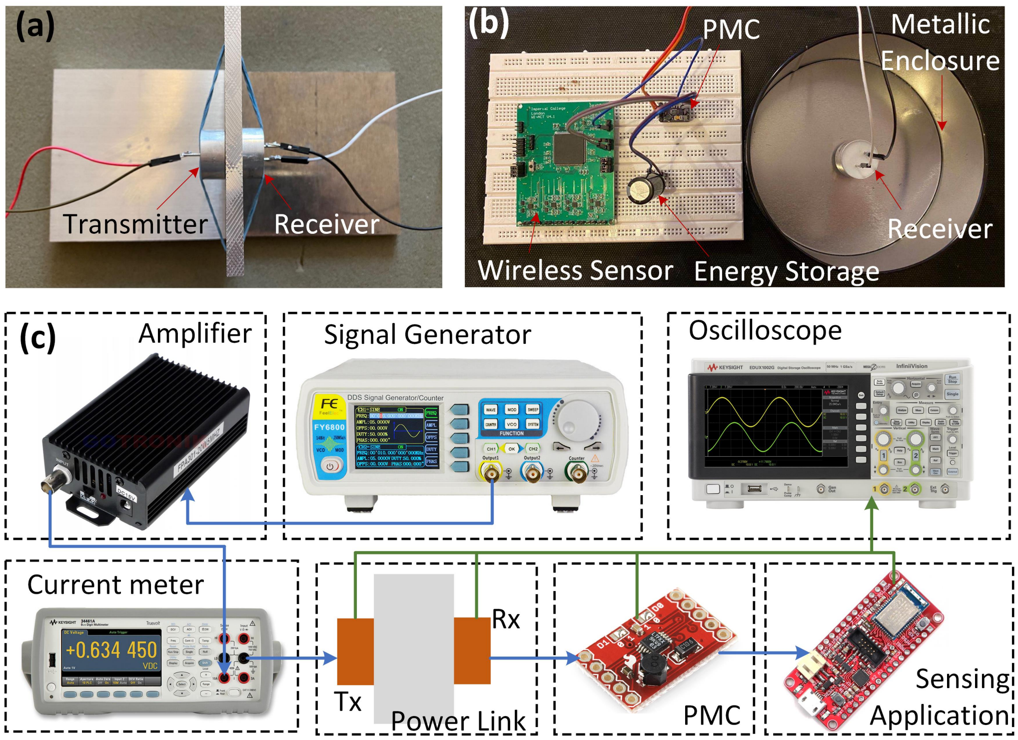

Figure 4: Experimental setup. (a) Simplified UWPL setup using an aluminium plate to verify the medium thickness influence; (b) UWPL for enclosed metallic structures with power management and sensing subsystems and (c) the overall experimental setup for testing and measurement.

enclosure with a transmitter placed on the opposite side of the enclosure. The received energy from the PZT Rx is directly regulated by a PMC using the LTC 35888-1 chip, where the AC power is rectified and converted into a constant DC output. The chip is fully powered by the received energy from the PZT Rx without using additional batteries. A 1 mF capacitor was adopted to store the energy received by the UWPL. A power readiness indicator is also generated by a built-in comparator in the PMC. A wireless sensor node with a micro-controller, accelerometers and a wireless module was adopted to examine the power transfer capability.

The overall testing platform is illustrated in Fig. 4(c). In order to implement the UWPL, a signal generator is necessary to provide the necessary signal for the proposed actuation. The FY6800 model from Feeltech was chosen to provide signals (up to 60 MHz). A power amplifier FPA301 from Feeltech was used to amplify the voltage provided by the generator and enhance the actuation capability. Then a multi-meter 34461A from Keysight was connected in series with the amplifier to quantify the current consumption. The actuation signal is then applied on the transmitter in Fig. 4(a). The transferred energy at the receiver end is then regulated by the PMC and stored in the capacitor for the subsequent sensing applications. The voltages on the transmitter, receiver and the energy storage were measured by an oscilloscope.

3.2. Finite Element Analysis using COMSOL

To visualize and analyze the interaction of PZTs with aluminium plates, ultrasonic waves were simulated based on a finite element software, COMSOL Multiphysics. The plates and PZTs used in the experiments were 2D modeled using Structural Mechanics Module with Piezoelectric Solid Interaction physics. The material of the plate and PZT discs were selected as Al-1050 and PZT-8, respectively. The actuating PZT with the diameter of 9 mm and thickness of 0.35 mm without the aluminium housing attached to the plates were actuated by the input sinusoidal signal with a central frequency of 39.8 kHz. The amplitude increases linearly from 1.5 V to 15 V to match the experimental input amplitude so that the results can be easily compared. The signal was applied to the PZT-8 face as an electrical potential.

4. Results and Discussions

4.1. Power Transfer via Aluminium Plates

For the convenience of testing the performance of the UWPL in different conditions, aluminium plates with different thicknesses were used in the first place. An actuation signal at 42.6 kHz was applied on the transmitter. The voltage amplitude increases linearly from 1 V to 15 V over a period of 20 s in order to check the capability of the system under different excitation voltage amplitudes, as shown in Fig. 5(a). Fig. 5(b) is the open-circuit voltage of the receiver, and the voltage varies from 0.2 V to 3.5 V due to the transmitter actuation. It can be seen that over a 6 mm thick aluminium plate, the received voltage has been attenuated by a ratio around 0.23. This ratio can be enhanced by either reducing the thickness of the medium or increasing the dimensions of the transmitter. As shown in Eq. (12), the received voltage V_s determines the energy can be used for the subsequent sensing applications.

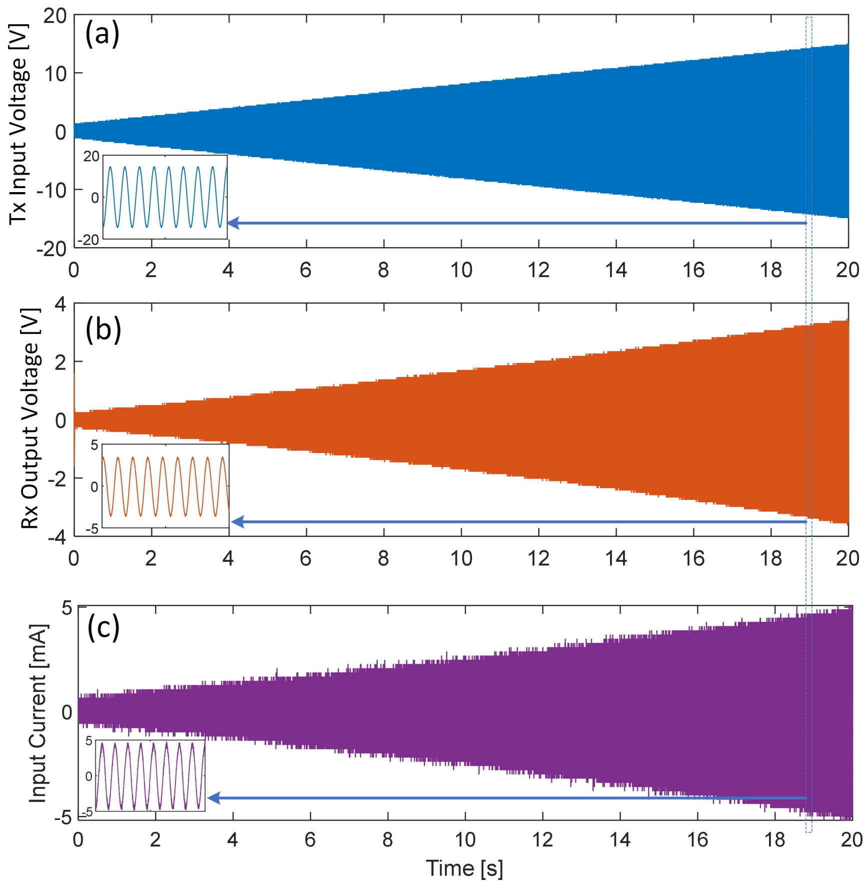

Figure 5: Power transfer capability of the power link through an 6 mm thick aluminium plate for different actuation amplitudes at 42.6 kHz. (a) Voltage applied on the piezoelectric transmitter; (b) open-circuit voltage on the receiver; (c) current consumption of the transmitter for varying voltage input.

Increasing the transmitter actuation voltage is the solution to increasing the received power. Fig. 5(c) is the AC current passing through the transmitter. The current consumption follows the increase of the applied actuation voltage. Based on the results in Fig. 5(a) and Fig. 5(c), the input RMS power P_{in} varies from 0.1 mW to 8.8 mW. As the input power increases exponentially with the voltage enhancement, using higher actuation voltage can be the solution to increasing the input power and the resultant received power significantly.

A frequency sweep test was conducted to examine the frequency-domain

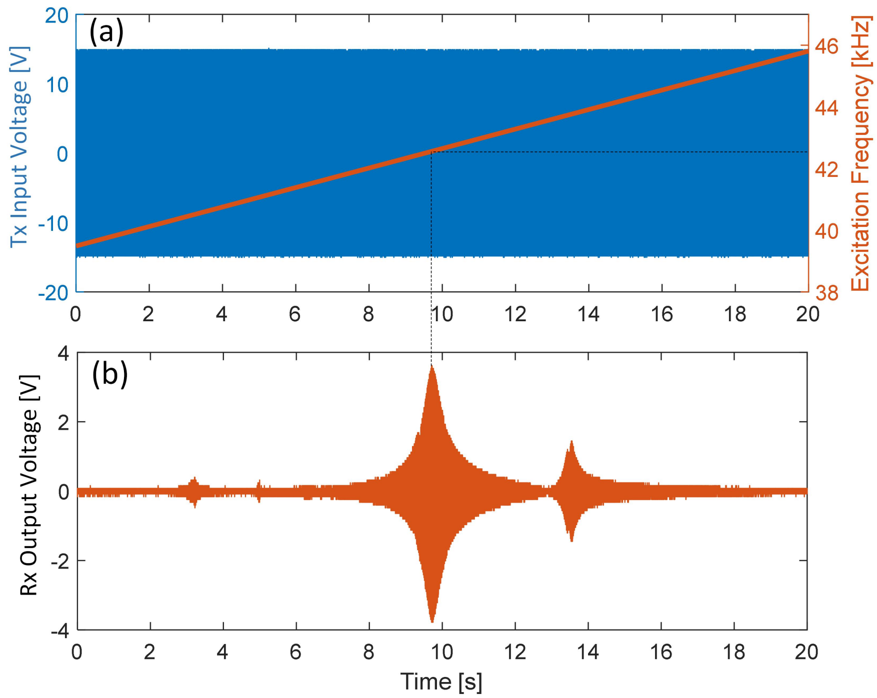

Figure 6: Power transfer capability of the power link through an aluminium plate for different actuation frequencies at 15 V. (a) Voltage applied on the piezoelectric transmitter with different frequencies; (b) open-circuit output voltage on the receiver.

characteristics of the UWPL, and the results are shown in Fig. 6. The excitation amplitude is 15 V and the excitation frequency increases linearly from 40 kHz to 46 kHz, as shown in Fig 6(a). The receiver response for different excitation frequencies is illustrated in Fig. 6(b). Multiple peaks co-exist with the peak at 42.6 kHz being the highest. This resonant frequency is different from the transducer's resonant frequency (40 kHz). The difference may originate from the effect of the transducer path, or the contacts between the transducers and the medium. The overall power link resonant frequency 42.6 kHz should be equal to the excitation frequency for the applied voltage in order to obtain the highest power transfer capability. In practice, the system central frequency can be identified by monitoring the current variation passing thought the PZT Tx and the central frequency is obtained when the current is the maximum.

To examine the output impedance of the UWPL, pure resistive loads were

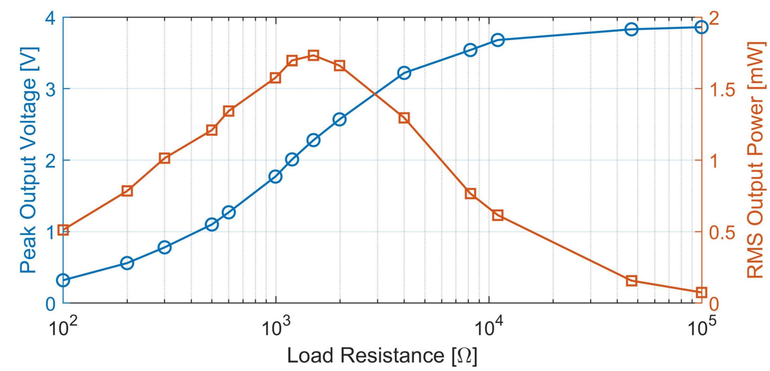

Figure 7: RMS Output power and peak output voltage of the receiver with different resistive loads for 15 V and 43.9 kHz input excitation.

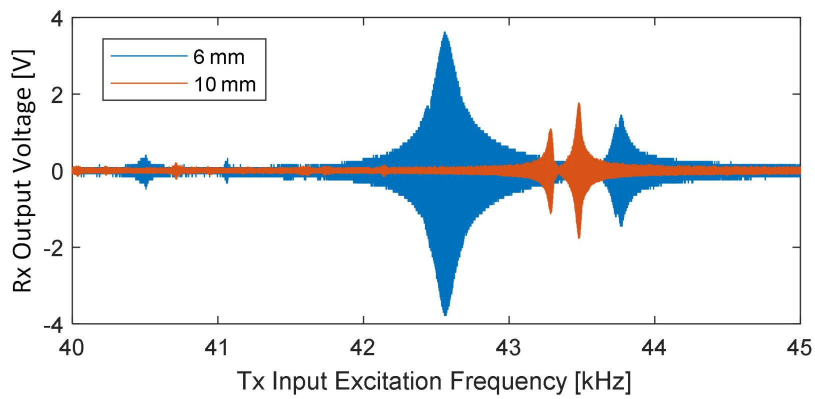

Figure 8: Energy transfer capability versus medium thickness for different input excitation frequencies and 15 V amplitude.

directly connected to the receiver to measure the power consumed by the loads. The output power and voltage are shown in Fig. 7. The optimal load resistance is about 1.5 kΩ with the highest output power of 1.73 mW. The energy efficiency of the power link under this operation condition is 19.7% (1.73/8.8). It is worth noting that an inductive load can be used to obtain electric impedance matching and enhance the power transfer performance. For simplicity, a resistive load is adopted in this study, but more solutions on how to include the inductive load in the matching network can be found in Refs [52, 53].

The influence of the metallic barrier thickness was examined experimentally for two aluminium plates with the thickness of 6 mm and 10 mm at different excitation frequencies, as shown in Fig. 8. With the increase of the medium thickness, the obtainable power by the receiver reduces, which agrees with the theoretical model in Eq. (9). It can be seen that the resonant frequencies for these two cases are different, although the same transducers were used in these tests. The variation was the medium thickness and contact conditions between the medium and the transducers. In terms of the received output voltage, the medium thickness affects the obtainable voltage significantly from 3.45 V with the 6 mm thick plate to 1.32 V with the 10 mm thick plate when the input excitation voltage is 15 V at resonance.

Then, the UWPL was tested under different excitation amplitudes at their resonant frequencies, as shown in Fig. 9(a). The input excitation voltage for the PZT Tx increases linearly from 1.5 V to 15 V, and a proportional output voltage was obtained from the receiver. The gap between the TX and Rx has a significant impact on the power transfer capability, and increasing the input excitation voltage is the straightforward solution when a larger output voltage is needed over a thick metallic medium. The results from the finite element model in COMSOL are included in Fig. 9(b) to provide a comparison to the experimental results. A good match in both the trend and amplitude for different aluminium plate thickness values is presented.

4.2. Power Management Circuit

For UWPL, the output is in AC form and needs to be rectified to be used for sensing applications. Based on the function description in Fig. 3, the power management chip LTC 3588-1 was chosen to regulate the AC input from the piezoelectric receiver into a constant 3.6 V output for sensing applications. A rectification module, a DC-DC conversion module and a comparator module to provide an enabling signal are included in this chip. A 1 mF capacitor was used to store the regulated energy, and the enclosed metallic structure shown in Fig. 4(b) was used in this test.

Fig. 10 shows the process of the charging and discharging cycles of the capacitor using the power management chip. The capacitor was charged to 3.7 V from zero in about 60 s with the stored energy of 6.8 mJ and the average power of 114 μW. A power readiness indicator (enabling signal) presents a pulse with the amplitude of 3.7 V and the duration of 0.3 s, as shown in Fig. 10(b). This pulse can be used as a trigger to enable the subsequent sensing module. Here, a 11 kΩ resistor was used to discharge the capacitor. It takes 20 s for the capacitor to decrease from 3.7 V to 1 V. Accordingly,

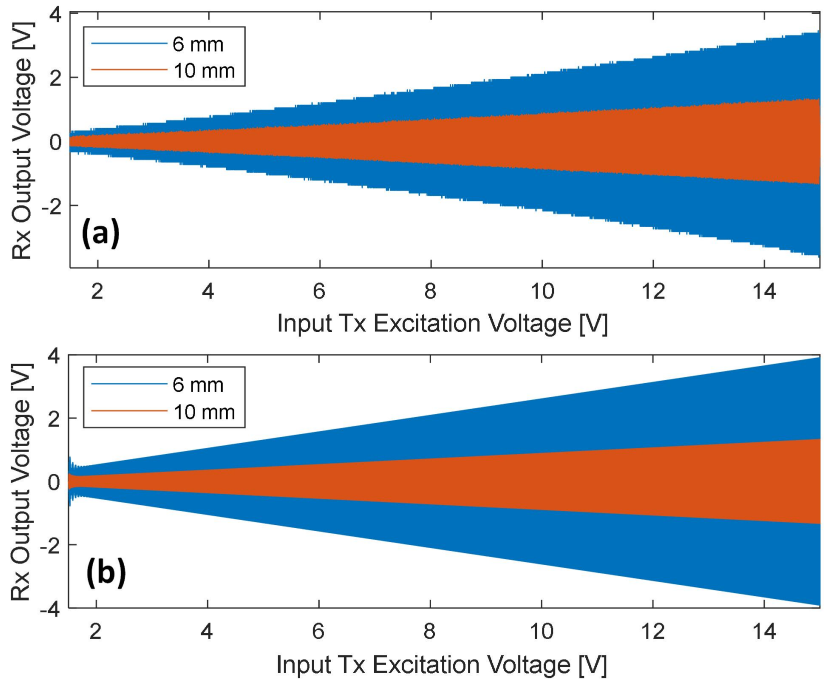

Figure 9: Energy transfer capability versus medium thickness. (a) experimental results and (b) Comsol simulation results.

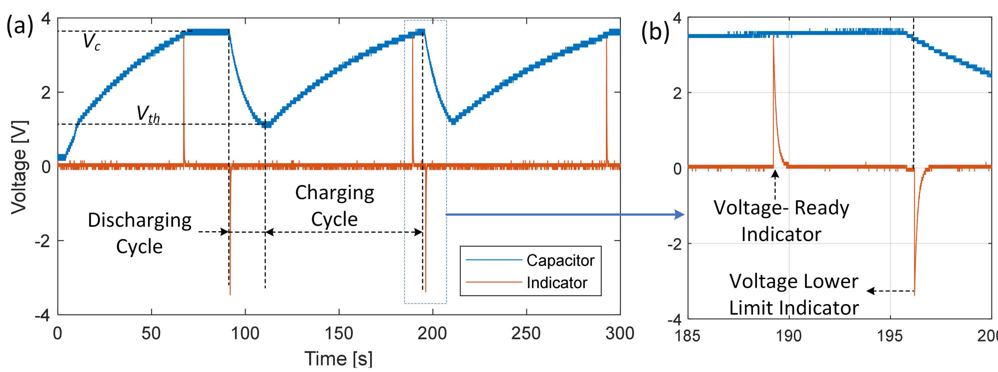

Figure 10: Performance of the power management circuit for charging and discharging. (a) Capacitor voltage and power readiness indicator for charging and discharging cycles and (b) enlarged view of the dished box in (a), showing the details of the power readiness indicator.

385 the consumed energy and average power are 6.3 mJ and 577 μW. Then,

Table 1: Power consumption of an example wireless sensor node.

Module	Mode	Current	Duration
MCU	Active	5 mA	τ_c
	Shut-down	1 μA	τ_s
Wireless	Transceiving	5 mA	τ_a
	Sleep mode	0.5 μA	$\tau_c + \tau_s - \tau_a$
Sensing	Active	2 mA	τ_{se}
	Shut-down	0.5 μA	$\tau_c + \tau_s - \tau_{se}$
Summary	Active	12 mA	τ_c
	Waiting	2 μA	τ_s

the recharging cycle restarts. The discharging is controlled by the sensing modules and can be initiated by the trigger signal and terminated when a certain duration (e.g. 10 s) is reached.

4.3. Energy Budget Balance Analysis

A balance between the UWPL power transfer capability and sensing power requirement is critical to maintain the operation of sensing applications. The energy budget balance analysis is discussed here. The power consumption of a typical wireless sensor node is summarized in Table 1. According to the power consumption requirement, the storage capacitance, charging time and the power transfer requirement can be determined using the theoretical model (Eq. 13) introduced in Section 2. As shown in Table 1, the power consumption in the active mode is the major power consuming element. Therefore, the energy balance analysis is based on the different sensing operation duration τ_c requirement for the active mode.

Fig. 11 illustrates the required energy storage capacitance and the needed charging time for different sensing currents and duration. The capacitance is primarily determined by the sensing current consumption and duration. The capacitance increases linearly with the rise of sensing active currents and duration, as shown in Fig. 11(a). In terms of the charging duration, it is co-determined by the needed energy and the charging capability of the UWPL. According to the experimental results in Fig. 5, the charging capability increases with the enhancement of the input voltage. 6.5 V output voltage at the receiver was used in the experiment and the average input power for the energy storage was measured as 1.4 mW. Based on these results, the required charging duration is calculated, as shown in Fig. 11(b).

Longer charging time are needed if the sensing active current and duration increases. However, increasing the power transfer capability is the solution to reducing the charging time.

5. Conclusions

In this paper, a system-level battery-free power supply solution for monitoring of metallic enclosures is developed using ultrasonic wireless power links enabled by piezoelectric transducers, power management circuits and sensing electronics. The ultrasonic wireless power link is designed, modelled and experimentally studied to transfer energy through metallic structures. In such a power link, one piezoelectric transducer is used as the transmitter to generate ultrasonic waves which can penetrate thick metallic structures, and another piezoelectric transducer is used as the receiver mounted on the other side of the metallic barrier to collect the transmitted ultrasonic energy. A theoretical model is developed to study the power transfer dynamics and analyse the power budget balance between the power transfer capability and the sensing power requirement.

The ultrasonic power transfer system is then validated experimentally. Different tests, including frequency and amplitude sweep tests, impedance matching tests, and medium thickness influence tests were carried out to evaluate the system performance. 1.73 mW output power was obtained on a 1.5 kΩ resister with the input voltage of 15 V at 42.6 kHz through a 6

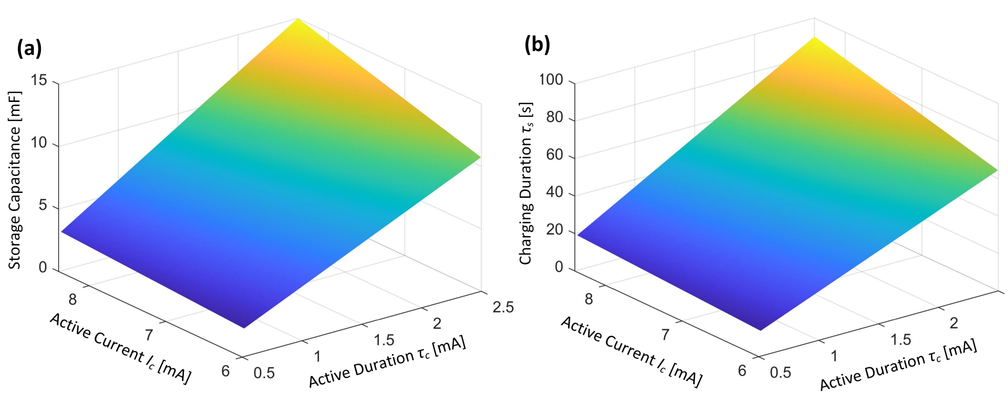

Figure 11: Energy balance analysis between sensing requirements and power transfer capability. (a) Storage capacitance as functions of sensing system operation duration and current requirement and (b) charging time as functions of sensing duration and current.

mm-thick aluminum plate. Different transfer distances were studied, showing that the received energy reduces significantly if the distance increases. A comparison with the simulation results shows a good match. A power management circuit was presented and tested to establish the system-level power supply solution for embedded sensing solution. A 1 mF capacitor was fully charged to 3.7 V from zero in about 60 s with the stored energy of 6.8 mJ and the average power of 114 μW. An energy balance analysis was conducted to examine the power transfer and management requirements for particular sensing power demand conditions.

The ultrasonic wireless power link presented in this work exhibits its capability in energizing embedded condition monitoring sensors through metallic medium, providing solutions for autonomous battery-free sensing in long-term monitoring of metallic structures, such as pipelines, airframe or nuclear waste container without human involvement.

References

[1] T. Wang, Q. Han, F. Chu, Z. Feng, Vibration based condition monitoring and fault diagnosis of wind turbine planetary gearbox: A review, Mechanical Systems and Signal Processing 126 (2019) 662–685.

[2] L. Ye, Study on embedded system in monitoring of intelligent city pipeline network, Computer Communications 153 (2020) 451–458.

[3] R. Gorgin, Y. Luo, Z. Wu, Environmental and operational conditions effects on lamb wave based structural health monitoring systems: A review, Ultrasonics (2020) 106114.

[4] F. P. G. Márquez, I. S. Ramírez, Condition monitoring system for solar power plants with radiometric and thermographic sensors embedded in unmanned aerial vehicles, Measurement 139 (2019) 152–162.

[5] C. Andreades, G. P. M. Fierro, M. Meo, A nonlinear ultrasonic shm method for impact damage localisation in composite panels using a sparse array of piezoelectric pzt transducers, Ultrasonics (2020) 106181.

[6] B. Warneke, M. Last, B. Liebowitz, K. S. Pister, Smart dust: Communicating with a cubic-millimeter computer, Computer 34 (2001) 44–51.

[7] L. Niccolai, M. Bassetto, A. A. Quarta, G. Mengali, A review of smart dust architecture, dynamics, and mission applications, Progress in Aerospace Sciences 106 (2019) 1–14.

[8] S. Yuan, Y. Ren, L. Qiu, H. Mei, A multi-response-based wireless impact monitoring network for aircraft composite structures, IEEE Transactions on Industrial Electronics 63 (2016) 7712–7722.

[9] A. Ozdagli, B. Liu, F. Moreu, Low-cost, efficient wireless intelligent sensors (lewis) measuring real-time reference-free dynamic displacements, Mechanical Systems and Signal Processing 107 (2018) 343–356.

[10] P. D. Mitcheson, E. M. Yeatman, G. K. Rao, A. S. Holmes, T. C. Green, Energy harvesting from human and machine motion for wireless electronic devices, Proceedings of the IEEE 96 (2008) 1457–1486.

[11] M. Luo, H. Luo, D. Axinte, D. Liu, J. Mei, Z. Liao, A wireless instrumented milling cutter system with embedded pvdf sensors, Mechanical Systems and Signal Processing 110 (2018) 556–568.

[12] N. Testoni, F. Zonzini, A. Marzani, V. Scarponi, L. De Marchi, A tilt sensor node embedding a data-fusion algorithm for vibration-based shm, Electronics 8 (2019) 45.

[13] J.-M. Dilhac, M. Bafleur, Energy harvesting in aeronautics for battery-free wireless sensor networks, IEEE Aerospace and Electronic Systems Magazine 29 (2014) 18–22.

[14] H. Fu, E. M. Yeatman, Rotational energy harvesting using bi-stability and frequency up-conversion for low-power sensing applications: Theoretical modelling and experimental validation, Mechanical Systems and Signal Processing 125 (2019) 229–244.

[15] F. Yang, L. Du, W. Chen, J. Li, Y. Wang, D. Wang, Hybrid energy harvesting for condition monitoring sensors in power grids, Energy 118 (2017) 435–445.

[16] S. Ozeri, D. Shmilovitz, Simultaneous backward data transmission and power harvesting in an ultrasonic transcutaneous energy transfer link employing acoustically dependent electric impedance modulation, Ultrasonics 54 (2014) 1929–1937.

[17] A. P. Sample, D. T. Meyer, J. R. Smith, Analysis, experimental results, and range adaptation of magnetically coupled resonators for wireless power transfer, IEEE Transactions on industrial electronics 58 (2010) 544–554.

[18] M. Salas, O. Focke, A. S. Herrmann, W. Lang, Wireless power transmission for structural health monitoring of fiber-reinforced-composite materials, IEEE Sensors Journal 14 (2014) 2171–2176.

[19] Z. Zhang, A. Georgiadis, C. Cecati, Wireless power transfer for smart industrial and home applications, IEEE Transactions on Industrial Electronics 66 (2019) 3959–3962.

[20] S. Ozeri, D. Shmilovitz, Ultrasonic transcutaneous energy transfer for powering implanted devices, Ultrasonics 50 (2010) 556–566.

[21] J. Wang, W. Zhao, Z. Su, G. Zhang, P. Li, D. Yurchenko, Enhancing vortex-induced vibrations of a cylinder with rod attachments for hydrokinetic power generation, Mechanical Systems and Signal Processing 145 (2020) 106912.

[22] J. Silva-Leon, A. Cioncolini, M. R. Nabawy, A. Revell, A. Kennaugh, Simultaneous wind and solar energy harvesting with inverted flags, Applied Energy 239 (2019) 846–858.

[23] G. A. Covic, J. T. Boys, Modern trends in inductive power transfer for transportation applications, IEEE Journal of Emerging and Selected topics in power electronics 1 (2013) 28–41.

[24] A. Danilov, E. Mindubaev, S. Selishchev, Methods for compensation of coil misalignment in systems for inductive transcutaneous power transfer to implanted medical devices, Biomedical Engineering 51 (2017) 56–60.

[25] X. Mou, D. T. Gladwin, R. Zhao, H. Sun, Survey on magnetic resonant coupling wireless power transfer technology for electric vehicle charging, IET Power Electronics 12 (2019) 3005–3020.

[26] L. Olvitz, D. Vinko, T. Švedek, Wireless power transfer for mobile phone charging device, in: 2012 Proceedings of the 35th International Convention MIPRO, IEEE, 2012, pp. 141–145.

[27] J. M. Arteaga, S. Aldhaher, G. Kkelis, C. Kwan, D. C. Yates, P. D. Mitcheson, Dynamic capabilities of multi-mhz inductive power transfer systems demonstrated with batteryless drones, IEEE Transactions on Power Electronics 34 (2018) 5093–5104.

[28] H.-J. Kim, H. Hirayama, S. Kim, K. J. Han, R. Zhang, J.-W. Choi, Review of near-field wireless power and communication for biomedical applications, IEEE Access 5 (2017) 21264–21285.

[29] G. Wang, W. Liu, M. Sivaprakasam, G. A. Kendir, Design and analysis of an adaptive transcutaneous power telemetry for biomedical implants, IEEE Transactions on Circuits and Systems I: Regular Papers 52 (2005) 2109–2117.

[30] M. M. Ahmadi, S. Ghandi, A class-e power amplifier with wideband fsk modulation for inductive power and data transmission to medical implants, IEEE Sensors Journal 18 (2018) 7242–7252.

[31] D. E. Boyle, S. W. Wright, M. E. Kiziroglou, A. Y. Pandiyan, E. M. Yeatman, Inductive power delivery with acoustic distribution to wireless sensors, in: 2019 IEEE PELS Workshop on Emerging Technologies: Wireless Power Transfer (WoW), IEEE, 2019, pp. 202–204.

[32] H. Basaeri, D. B. Christensen, S. Roundy, A review of acoustic power transfer for bio-medical implants, Smart Materials and Structures 25 (2016) 123001.

[33] A. Denisov, E. Yeatman, Ultrasonic vs. inductive power delivery for miniature biomedical implants, in: 2010 International Conference on Body Sensor Networks, IEEE, 2010, pp. 84–89.

[34] Z. Sharif-Khodaei, M. Aliabadi, Assessment of delay-and-sum algorithms for damage detection in aluminium and composite plates, Smart materials and structures 23 (2014) 075007.

[35] J. Charthad, M. J. Weber, T. C. Chang, A. Arbabian, A mm-sized implantable medical device (imd) with ultrasonic power transfer and a hybrid bi-directional data link, IEEE Journal of solid-state circuits 50 (2015) 1741–1753.

[36] D. Seo, R. M. Neely, K. Shen, U. Singhal, E. Alon, J. M. Rabaey, J. M. Carmena, M. M. Maharbiz, Wireless recording in the peripheral nervous system with ultrasonic neural dust, Neuron 91 (2016) 529–539.

[37] M. Alam, S. Li, R. U. Ahmed, Y. M. Yam, S. Thakur, X.-Y. Wang, D. Tang, S. Ng, Y.-P. Zheng, Development of a battery-free ultrasonically powered functional electrical stimulator for movement restoration after paralyzing spinal cord injury, Journal of NeuroEngineering and Rehabilitation 16 (2019) 36.

[38] L. Radziemski, I. R. S. Makin, In vivo demonstration of ultrasound power delivery to charge implanted medical devices via acute and survival porcine studies, Ultrasonics 64 (2016) 1–9.

[39] A. Allam, K. G. Sabra, A. Erturk, Aspect ratio-dependent dynamics of piezoelectric transducers in wireless acoustic power transfer, IEEE Transactions on Ultrasonics, Ferroelectrics, and Frequency Control 67 (2019) 984–996.

[40] H. Vihvelin, J. R. Leadbetter, M. Bance, J. A. Brown, R. B. Adamson, Compensating for tissue changes in an ultrasonic power link for implanted medical devices, IEEE transactions on biomedical circuits and systems 10 (2015) 404–411.

[41] C. Paraskevoulakos, C. Stitt, K. Hallam, A. Banos, M. L. Olloqui, C. Jones, G. Griffiths, A. Adamska, J. Jowsey, T. Scott, Monitoring the degradation of nuclear waste packages induced by interior metallic corrosion using synchrotron x-ray tomography, Construction and Building Materials 215 (2019) 90–103.

[42] S. Delvecchio, P. Bonfiglio, F. Pompoli, Vibro-acoustic condition monitoring of internal combustion engines: A critical review of existing techniques, Mechanical Systems and Signal Processing 99 (2018) 661–683.

[43] K. Wang, Z. Liu, X. Qian, Y. He, Dynamic characteristics and damage recognition of blast-induced ground vibration for natural gas transmission pipeline and its integrated systems, Mechanical Systems and Signal Processing 136 (2020) 106472.

[44] M. Kiziroglou, D. Boyle, S. Wright, E. Yeatman, Acoustic power delivery to pipeline monitoring wireless sensors, Ultrasonics 77 (2017) 54–60.

[45] J. D. Ashdown, K. R. Wilt, T. J. Lawry, G. J. Saulnier, D. A. Shoudy, H. A. Scarton, A. J. Gavens, A full-duplex ultrasonic through-wall communication and power delivery system, IEEE transactions on ultrasonics, ferroelectrics, and frequency control 60 (2013) 587–595.

[46] D.-X. Yang, Z. Hu, H. Zhao, H.-F. Hu, Y.-Z. Sun, B.-J. Hou, Through-metal-wall power delivery and data transmission for enclosed sensors: A review, Sensors 15 (2015) 31581–31605.

[47] R. Krimholtz, D. A. Leedom, G. L. Matthaei, New equivalent circuits for elementary piezoelectric transducers, Electronics Letters 6 (1970) 398–399.

[48] S. H. Song, A. Kim, B. Ziaie, Omnidirectional ultrasonic powering for millimeter-scale implantable devices, IEEE Transactions on Biomedical Engineering 62 (2015) 2717–2723.

[49] Y. Wang, Y. Xia, Recent progress in supercapacitors: from materials design to system construction, Advanced materials 25 (2013) 5336–5342.

[50] Y. Liu, E. Liu, Y. Chen, X. Wang, C. Sun, J. Tan, Measurement of fastening force using dry-coupled ultrasonic waves, Ultrasonics 108 (2020) 106178.

[51] R. Hou, Y. Q. Fu, D. Hutson, C. Zhao, E. Gimenez, K. J. Kirk, Use of sputtered zinc oxide film on aluminium foil substrate to produce a flexible and low profile ultrasonic transducer, Ultrasonics 68 (2016) 54–60.

[52] H. Huang, D. Paramo, Broadband electrical impedance matching for piezoelectric ultrasound transducers, IEEE transactions on ultrasonics, ferroelectrics, and frequency control 58 (2011) 2699–2707.

[53] V. T. Rathod, A review of electric impedance matching techniques for piezoelectric sensors, actuators and transducers, Electronics 8 (2019) 169.